Indian Journal of Chemical Technology
Vol. 30, November 2023, pp. 789-796
DOI: 10.56042/ijct.v30i6.4392

An investigation of characteristics of a diesel engine with low heat rejection fuelled by spirulina algae biodiesel

J Arunprasad[1], S Karthikeyan[2]* & Arif Senol SENER[3]

[1]Department of Mechanical Engineering, Dhanalakshmi Srinivasan Engineering College, Tamil Nadu, India
[2]Department of Mechanical Engineering, Syed Ammal Engineering College, Tamil Nadu, India
[3]Department of Mechanical Engineering, Engineering and Architecture Faculty, Nisantasi University, Istanbul, Turkey
*E-mail: skarthikeya74@gmail.com (SK)

Received 28 July 2023; accepted 28 September 2023

This study investigates the impact of magnesium oxide nanoparticles on the performance, combustion, and emissions characteristics of spirulina algae methyl ester biodiesel in a low heat rejection (LHR) engine. The cylinder head and piston of the engine are coated with a 200-micron layer of lanthanum aluminate. The results indicate promising outcomes with biodiesel in the LHR engine, showing improved thermal efficiency and reduced specific fuel consumption compared to conventional diesel engines. Tests have been conducted on B20, B20+25 ppm of MgO, and B20+50 ppm of MgO biodiesel blends with coated and untreated components. The coated piston with B20+50 ppm of MgO (LHR) demonstrate a 1.73% increase in brake thermal efficiency and a 7.2% decrease in specific fuel consumption compared to an untreated piston. Furthermore, the B20+50 ppm of MgO (LHR) in B20 experience a 5.9% reduction in-cylinder pressure and a 6.9% decrease in heat release rate. Additionally, the coated engine exhibit lower CO, HC, and smoke emissions from the biodiesel blends than the conventional engine.

Keywords: Biodiesel engine, Emission characteristics, Low heat rejection engine, Magnesium oxide biodiesel blend, Spirulina algae methyl ester

Due to a rise in crude oil prices, increasing population and environmental concerns, many researchers focus on alternative fuels. Biodiesel is an alternative source of conventional fossil fuel, which is renewable, nontoxic, and biodegradable. Mono-alkyl ester present in biodiesel is generally produced from renewable feedstock. Vegetable oils for biodiesel can be obtained from edible or non-edible feedstocks[1]. In Europe and the USA, surplus vegetable oils are utilized for biodiesel. But there is a debate regarding using edible feedstock as an automotive fuel. This may create an imbalance in the world's food supply and demand chain. In addition, edible oil resources are expensive to use as biodiesel sources, and their production is not economically feasible. Consequently, edible oil resources are not encouraged. In India, several non-edible seed plants bear vegetable oils such as jatropha, karanja, yellow oleander, pomelo, rubber, tea, neem, nahor, rattan jot, lemongrass, cotton, mahua, pongamia, etc.[2] biodiesel has some limitations. The main disadvantages of biodiesel in diesel engines are poor atomization and vapourisation, high smoke, and sticky deposits on engine elements because of its high viscosities. These issues are often overcome by adopting appropriate ways like blending, changing to biodiesel, heating to reduce viscosity, low heat rejection (LHR) of diesel engines, fuel additives, etc. Several engine modifications have been explored, with LHR engine being one of the most viable options. Plasma spraying is the commonly employed technique for applying these coatings, allowing selective application to key engine components like valves, cylinder heads, piston crowns, and the entire combustion chamber. The main aim is to minimize the heat loss through the chamber walls to the cooling system, thus converting more energy into useful work within the cylinder. As a result, this enhances engine efficiency and reduces emissions[3]. LHR engines have significant advantages such as a decrease in ignition delay, uniform heat distribution, decreased heat release rate, extended combustion duration, less increase in the cylinder pressure, increased life of the engine, and much more suitable for biodiesel operations. In addition, by incorporating nano additives into biodiesel, it is possible to enhance engine performance and reduce emissions[4].

This study aimed to investigate the impact of carbon nanotubes on a LHR diesel engine using waste plastic oil. The research analyzed low-heat rejection engines utilizing emulsion WPO20 with varying amounts of carbon nanotubes. The results showed significant reductions in smoke emissions (12.9%), hydrocarbon emissions (21.8%), and carbon monoxide emissions (22.7%) when 20 ppm of carbon nanotubes were added to WPO20, compared to regular diesel operation. Moreover, the LHR engine achieved a remarkable brake thermal efficiency of 31.7%, attributed to the improved emulsification and vapourization obtained with carbon nanotube doped WPO20[5]. Another aspect of the study involved practical and numerical experiments in evaluating the impact of yttria-stabilized zirconia coating and cerium oxide nano-additives on a cymbopoganflexuosus biofuel-powered diesel engine. The coated piston exhibited minimal thermal stress based on finite element analysis. Real-world experiments compared B20 (80% diesel + 20% biofuel) and B25 + C fuels (75% diesel + 25% biofuel with 20 ppm cerium nano-additives) in compression-ignition engines. The biofuel engine showed a 1.75% increase in efficiency due to reduced heat flux in the piston crown. Coated engines displayed higher heat release rates and in-cylinder pressure, leading to significant reductions of 55% in smoke, 4.75% in CO_2, and 3.63% in hydrocarbon emissions[6]. The engine's performance and emission characteristics were investigated using MEME20+25 ppm TiO_2, a mimusopselangi methyl ester fuel blend, and 25 ppm titanium oxide nanoparticles. The LHR engine featured a two-layer insulation coating on the piston crown, with a 50 µm NiCrAlY bond coat and a 250 µm topcoat containing 5% yttrium, 2% neodymium oxide, and 93% zirconium oxide applied via plasma spray. Compared to diesel fuel, notable improvements were observed: a 7.06% increase in brake thermal efficiency, a 16.38% decrease in brake-specific fuel consumption, and reductions of 35.66%, 31.8%, and 19.66% in carbon monoxide, hydrocarbon, and smoke emissions, respectively, however, at full load and 1500 rpm, nitrogen oxide emissions and exhaust gas temperature increased by 22.23% and 9.33%, respectively[7]. Another study evaluated the performance and emissions of cerium oxide nano-additives blended with palm biodiesel in engines with specific coatings. Plasma spray technology was employed to coat the engine combustion parts with a combination of PSZ and Al_2O_3 ceramic powder. The CeO_2 nano-additives were introduced at 30 and 60 ppm, respectively. The findings indicated significant improvements in engine performance. Compared to using pure palm biodiesel, adding CeO_2 at 30 ppm and 60 ppm increased the brake thermal efficiency by 3.21%, 4.28%, and 4.82%, respectively. Additionally, specific fuel consumption decreased by 11.86%, 16.92%, and 20.57%, respectively. There were reductions in carbon monoxide and hydrocarbon emissions, with decreases of 2.2% and 3.7%, respectively. However, nitrogen oxide emissions slightly increased by 1.7% for engines with thermal barrier coatings. Nevertheless, the use of cerium oxide nanoparticles as an oxygen-denoting catalyst led to a reduction in NO_x emissions by 2.4% [8]. After reviewing existing literature, it has been established that the LHR technique offers benefits such as improved engine performance, enhanced combustion efficiency, and reduced emissions. In this study, a thermal barrier coating of lanthanum aluminate using the plasma spraying technique was applied to achieve LHR. The diesel engine's piston crown and cylinder head were coated with a 200 µm layer of lanthanum aluminate. The main objective of this research was to evaluate the performance, combustion, and emissions characteristics of an LHR engine that utilized a combination of spirulina alage methyl ester with different concentrations of magnesium oxide. The findings obtained from this investigation were then compared to those of conventional engines to identify any discernible differences.

Experimental Section

Spirulina algae oil

Currently, algae are considered prospective biomass feedstock sources for manufacturing biofuels because of their exceptional biomass production compared to higher plants. Algae can be grown in non-arable lands and pitiable quality waters, which comprise seawater, brackish water, and industrial wastewater. The manufacturing of biodiesel from microalgae can be 10 to 20 times greater than the yield attained from seeds[9]. In addition, using microalgae in biofuel production is one of the most effective methods of removing CO_2 and can effectively reduce greenhouse gas emissions[10]. Spirulina is one of the oldest life forms on earth. Spirulina looks green and sometimes may turn bluish when scum is dying. The size of the Spirulina organism is between 300 to 500 microns.

Transesterification of spirulina algae biodiesel

The transesterification equipment includes a 5 L capacity round bottom flask with facilities for attaching a stirrer and thermometer for stirring and monitoring the temperature of the reactants. The catalyst solution was poured into the flask through an expanded neck provision. The bottom flask was supplied with an electric heating element for heating the reactants. The reactants in the flask were stirred using a motorized stirrer mounted on a stand with speed control. The alkaline transesterification technique converted spirulina oil into methyl ester using methanol with NaOH as a catalyst. 10 g NaOH was dissolved in 300 mL methanol and then mixed with vegetable oil to make 1 L of this mixture. The process of producing spirulina biodiesel involves: (i) heating the prepared solution to a temperature of 60°C, (ii) stirring the prepared mixture at 60°C for 30 min, (iii) pouring it into a separator and allowing the solution to cool to room temperature and layup for 8 - 12 h. The solution was separated from the glycerol found at the lower layer. The top film of methyl ester was moved into a glass container for further processing by mixing with the same amount of distilled H_2O. This biodiesel was heated to 100°C for 10 min to eliminate water particles and cooled down to ambient temperature before use.

Fuel samples

The dispersal of magnesium oxide nanoparticles into the B20 fuel sample was done in concentrations of 25 ppm with the help of an ultrasonicator. Table 1 compares the properties of various fuels, such as B20, B20+25 ppm of MgO and B20+50 ppm of MgO blend. It is mentioned in the table that the calorific value is lesser for B20 fuel than B20+25 ppm of MgO and B20+25 ppm of MgO.

Engine components coating using thermal barrier materials

Various properties of the lanthanum aluminate are compared with various thermal barrier coating materials presented in Table 2. Lanthanum aluminate has lesser thermal conductivity when compared with all other materials except for yttria-stabilized zirconia, which has higher thermal conductivity. Lanthanum aluminate has a higher thermal expansion coefficient, but yttria-stabilized zirconia and cerium oxide have a lesser thermal expansion coefficient. Lanthanum aluminate has a lesser density than all other materials except aluminium oxide, zirconium oxide, and barium zirconium oxide.

Plasma spraying technique

Plasma spraying technique was used to deposit coating material on combustion chamber elements. In this technique, at a higher temperature the surface melts, which is suitable for this method. The plasma spray process is shown in Fig. 1. The plasma spray solution system considers the powder feeding mechanism, gun and power supply, and gas sources. An arc is formed between a spray nozzle and an electrode. A plasma jet at a very high temperature of about >16000°C is passed between electrodes. The powder of deposited material will be given into the plasma jet. The particle velocity reaches 200-300 m/s for the deposition rate of 1-5 kg/h; it reduces the porosity to about 5 – 10% and the oxide content to about 1 – 3%. Towards the substrate, the materials are

Table 1 — Properties of various blends

Properties	B20	B20+25 ppm of MgO	B20+50 ppm of MgO
Kinetic viscosity (cSt)	5.3	6.01	6.12
Density (kg/m$^{3)}$	886	891	894
Cetane number	51	54	56
Calorific value (MJ/kg)	39.74	41.23	41.56
Flashpoint (^{o}C)	91	126	132
Fire point (^{o}C)	116	150	156

Table 2 — Different properties of thermal barrier coating materials

Properties	7-8% YSZ	CeO_2	Al_2O_3+40% ZrO_2	Ba ZrO_3	Lanthanum aluminate
Thermal conductivity (W/m K)	1	2.77	8	3.42	1.7
Thermal expansion coefficient (1/k) *10^{-6})	10.9	13	7.5	8.1	10.1
Density (kg/m^3)	5650	5253	4000	4200	4325

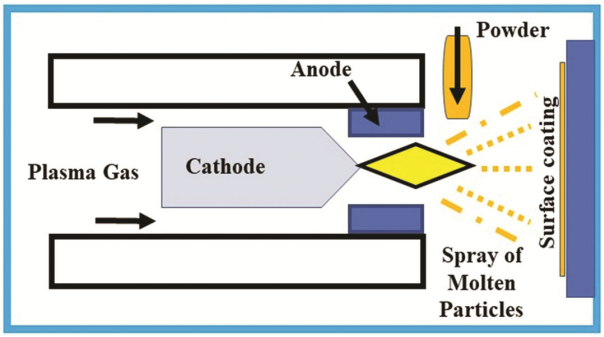

Fig. 1 — Schematic diagram of the plasma spray process

melted and propelled into the jet. Therefore, deposits are formed when flattening molten droplets solidify rapidly. The coated piston is shown in Fig. 2. White ceramic material lanthanum aluminate is used for coating, and 500 g were required for coating purposes. Engine combustion chamber elements are coated utilizing the plasma spraying technique. 100-120 PSI is the injecting pressure of the nozzle for argon, and for hydrogen, it is 50 PSI. The argon flow rate from the nozzle is 80-90 lpm, and the hydrogen flow rate is 15-18 lpm. 65-70 V is the developed voltage, and 500 amp current is developed. The powder is fed at 40-45 g/min, and the spray is 2-3 inches long. The plasma spraying process is the coating technique selected for obtaining a low heat rejection engine from the standard engine 200 microns thick coating was employed.

Uncertainty analysis

(i) Calculation of uncertainty in brake power

$$\frac{\Delta BP}{BP} = \left\{\left[\frac{\Delta W}{W}\right]^2 + \left[\frac{\Delta N}{N}\right]^2 + \left[\frac{\Delta R}{R}\right]^2\right\}^{1/2}$$

(ii) Calculation of uncertainty in fuel consumption

$$\frac{\Delta FC}{FC} = \left\{\left[\frac{\Delta V}{V}\right]^2 + \left[\frac{\Delta t}{t}\right]^2\right\}^{1/2}$$

(iii) Calculation of uncertainty in fuel power

$$\frac{\Delta FP}{FP} = \frac{\Delta FC}{FC} = \left\{\left[\frac{\Delta V}{V}\right]^2 + \left[\frac{\Delta t}{t}\right]^2\right\}^{1/2}$$

(iv) Calculation of uncertainty in Brake thermal efficiency

$$\frac{\Delta BTE}{BTE} = \left\{\left[\frac{\Delta BP}{BP}\right]^2 + \left[\frac{\Delta FC}{FC}\right]^2\right\}^{1/2}$$

Fig. 2 — Photographic view of lanthanum aluminate-coated surfaces of the cylinder piston

Total experimental uncertainty = Square root of {(uncertainty of TFC)^2 + (uncertainty of BP)^2 + (uncertainty of BSFC)^2 + (uncertainty of BTE)^2 + (uncertainty of CO)^2 + (uncertainty of HC)^2 + (uncertainty of Fuel measurement)^2 + (uncertainty of NO_X)^2 + (uncertainty of EGT indicator)^2 + (uncertainty of CO_2)^2+(uncertainty of O_2)^2+ (uncertainty of angle encoder) ^{2} + (uncertainty of pressure pick up)^2} = Square root of {(0.26)^2+(0.25)^2+ (0.25)^2+ (0.36)^2 +(0.1)^2+(0.1)^2+ (1)^2 + (0.2)^2 + (0.15)^2 + (0.15)^2+ (0.1)^2+ (0.2)^2 + (0.1)^2}.

Experimental setup

The tested engine was a single-cylinder, four-stroke, water-cooled compression ignition (CI) engine. At full load, it reached a maximum power output of 5.2 kW at 1500 rpm. The engine's compression ratio and displacement volumes are 17.5:1 and 661 cc, respectively. The fuel injector nozzle had an opening pressure of 210 bar, and the injection timing was 23° bTDC. A water jacket was integrated into the engine block to regulate the wall temperature to circulate coolant water around the walls of the combustion chamber. A high-speed eddy current dynamometer served as the loading device in the experimental setup. A piezoelectric sensor was attached to the engine head to measure in-cylinder gas pressure. HC, CO, and NO_x emissions were identified using the AVL-444 gas analyzer, while the AVL-437 smoke meter measured smoke opacity. Initially, the engine was run without load for a few minutes. Then, the test fuel loads were increased gradually at a constant rate of 1500 rpm, ranging from 0% to 100%. Fig. 3 presents the schematic diagram of the compression ignition engine experimental setup. Accuracy of the measuring instruments and percentage of uncertainties of engine parameters are given in Table 3 and Table 4, respectively.

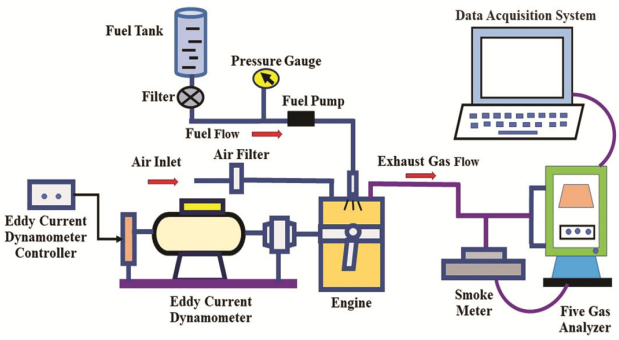

Fig. 3 — Schematic diagram for the experimental setup

Table 3 — Percentage of uncertainties of engine parameters

S. No.	Parameter	Percentage Uncertainties
1	FC	± 0.26
2	BTE	± 0.36
3	Fuel measurement	± 1
4	BP	± 0.25
5	O_2	± 0.1
6	HC	± 0.1
7	NO_x	± 0.2
8	CO	± 0.1

Table 4 — Accuracy of the measuring instruments

S. No.	Instrument		
1	Exhaust emission analyzer	CO: 0-10%	vol ± 0.01%
		HC:0-10000 ppm	± 10ppm
		CO_2 : 0-20%	vol ± 0.02 %
		NOx : 0-5000 ppm	± 10 ppm
		0 – 100%	± 1%
2	AVL Smoke meter	0 – 100%	± 1%

Results and Discussion

Brake specific fuel consumption

The engine's fuel efficiency was measured using specific fuel consumption. Fig. 4 illustrates the incremental reduction in specific fuel energy consumption of fuel blends at different loads. At maximum load, B20 fuel had a BSFC of 0.29 kg/kWh, while B20 (LHR), B20+25 ppm of MgO (LHR), and B20+50 ppm of MgO (LHR) fuel blends had values of 0.27 kg/kWh, 0.253 kg/kWh, and 0.231 kg/kWh, respectively. The reduction in BSFC for fuel blends can be attributed to the heat-trapping characteristic of the ceramic material, as well as the higher surface-to-volume ratio and improved energy transfer of nano additives[11]. These additives act as catalysts, releasing oxygen into the combustion chamber and promoting better combustion of spirulina biodiesel blends in the TBC engine[12]. The results show that the B20+50 ppm of MgO (LHR) fuel blend exhibited the lowest specific fuel consumption compared to other fuel blends.

Brake thermal efficiency

The amount of useful work performed by the chemical energy in the fuel is known as brake thermal efficiency, which illustrates how energy is converted. Fig. 5 shows the deviation in brake thermal efficiency with different loads for all the tested fuel blends. A significant improvement in BTE is observed for all biodiesel blends in the LHR engine at all loads. The results indicate that after coating the engine components, the brake thermal efficiency increased

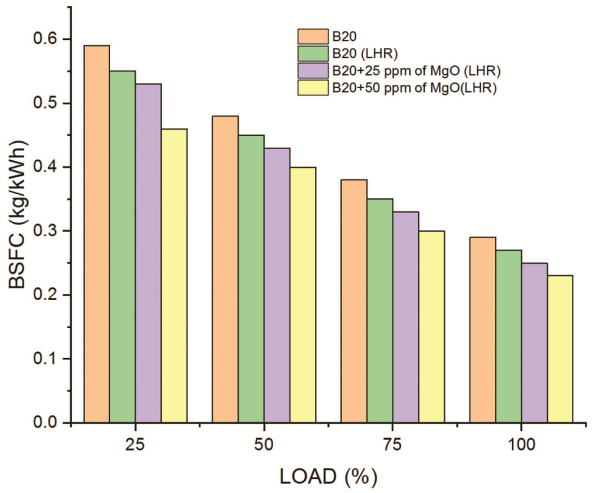

Fig. 4 — Plot of BSFC vs. load

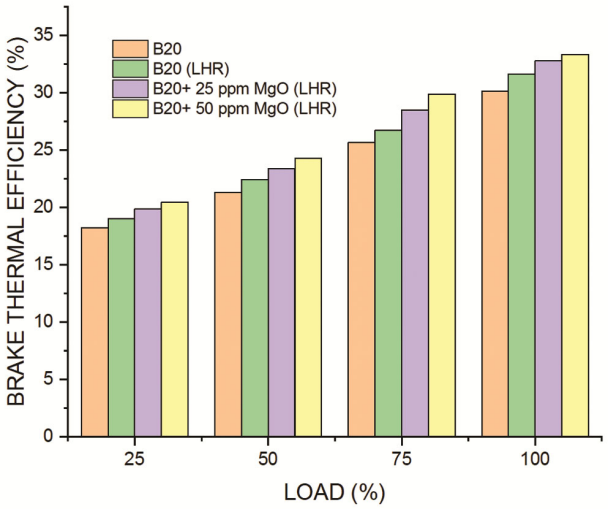

Fig. 5 — Plot of brake thermal efficiency vs. load

significantly for B20 with and without nano additives fuel blends. The B20 fuel blend also had a lower brake thermal efficiency range than other fuel blends. It was found that the B20+50 ppm of MgO (LHR) fuel blend produces 33.35% brake thermal efficiency at maximum load. This is 1.73% and 3.2% higher than B20+25 ppm of MgO (LHR) and B20 (LHR), respectively. Coating surfaces reduce heat loss and increase the cylinder temperature at all loads[13]. Furthermore, the MgO nanoparticles buffer oxygen content, influencing combustion processes, and enhancing brake thermal efficiency[14].

Heat release rate

The heat release rate relies on various factors, including fuel type, air-fuel ratio, and oxygen

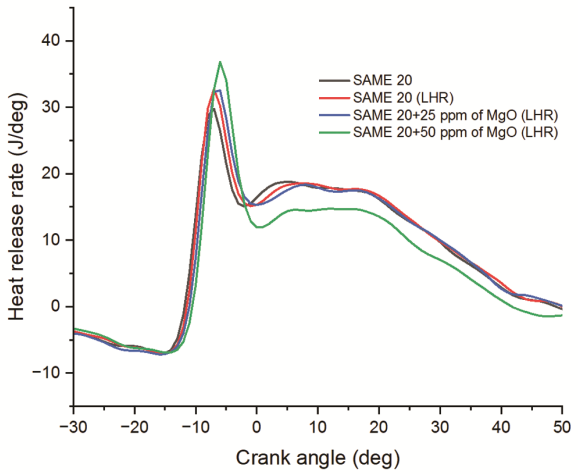

Fig. 6 — Heat release rate with respect to crank angle at full load

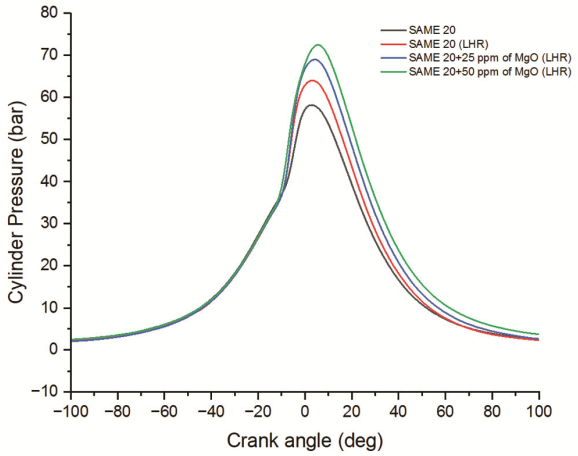

Fig. 7 — Cylinder pressure variation with respect to crank angle at full load

availability, all influencing it. Fig. 6 demonstrates the fluctuation of HRR for different crank angles with tested fuels. The coated engine exhibits the highest peak HRR for all tested fuels. Elevated temperatures and longer residence time in the cylinder result in improved fuel evaporation and atomization. The graph reveals that the B20 blend reduces the HRR of other fuel blends due to lower cylinder temperature and higher fuel viscosity. At maximum load, HRR for B20 fuel is 29 J/deg, while for B20 (LHR), B20+25 ppm of MgO (LHR), and B20+50 ppm of MgO (LHR) fuel blends, it's 31 J/deg, 33 J/deg, and 38 J/deg, respectively. Adding magnesium oxide nano-additives in B20 increases the HRR at maximum engine load, reducing the fuel's chemical delay and leading to higher HRR.

Cylinder pressure

Several factors can contribute to higher cylinder pressure, including fuel turbulence, viscosity, cetane number, and ignition delay. Additionally, combustion technology mainly focuses on peak pressure, which significantly affects the exhaust emissions of engines. Fig. 7 depicts the association between in-cylinder pressure and crank angle for all fuel blends. The graph indicates that the B20 fuel blend had a lower cylinder pressure range than other fuel blends. This lower pressure could be attributed to a reduced ability to evaporate fuel due to the high viscosity and density of the tested fuel blends, leading to a less efficient combustion process. The peak cylinder pressures at peak load from the engine are as follows: B20, B20 (LHR), B20+25 ppm of MgO (LHR), and B20+50 ppm of MgO (LHR) recorded at 58.66 bar, 64.12 bar, 69.31 bar, and 73.68 bar, respectively. Ceramic-coated engines can absorb thermal energy, improving cylinder pressure and temperature[15]. Moreover, nano additives increase the catalyst surface area and improve the fuel's oxygen capacity[16]. Among all other fuel blends, B20+50 ppm of MgO (LHR) dominates the plot at peak load.

Carbon monoxide

The air-to-fuel ratio significantly influences the amount of CO emitted by the test engine. CO emissions primarily occur due to a lack of oxygen during combustion. Controlling exhaust CO emissions is essential due to their poisonous nature. Fig. 8 illustrates the variation in carbon monoxide emissions for biodiesel blends with and without coatings under different loads. When using biodiesel blends, CO emissions from LHR engines decrease significantly under all conditions. At maximum load, the CO emissions observed for the B20 fuel were 0.077 g/kW-h, whereas, for the B20 (LHR), B20+25 ppm of MgO (LHR), and B20+50 ppm of MgO (LHR) fuel blends, they were 0.075 g/kW-h, 0.073 g/kW-h, and 0.07 g/kW-h, respectively. The LHR engine exhibits higher swirl velocity, turbulent kinetic energy, and excess oxygen in B20, leading to better combustion[17]. Furthermore, biodiesel contains MgO nanoparticles that promote homogeneous distribution and atomization, reducing carbon monoxide emissions[18].

Hydrocarbon emission

Hydrocarbon (HC) emissions mainly constitute the unburned or partially burned fuel particles generated due to inadequate temperature near the cylinder walls

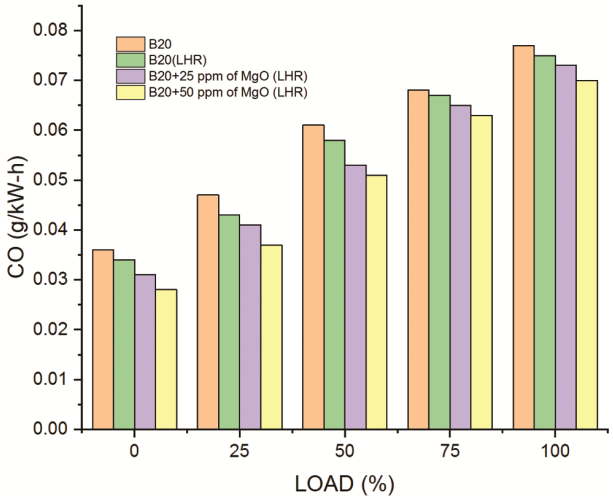

Fig. 8 — Plot of carbon monoxide emission vs. load

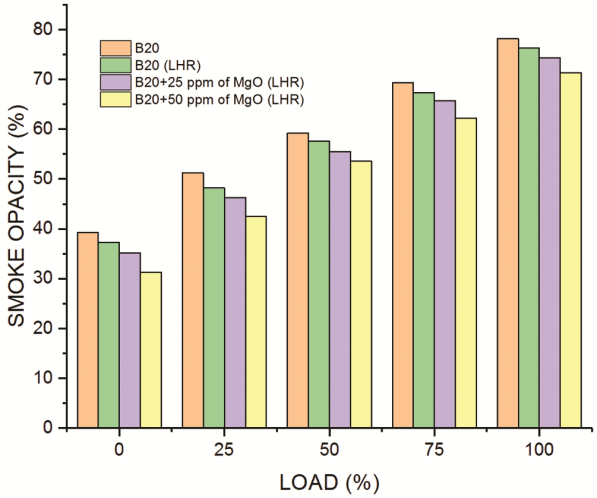

Fig. 10 — Plot of smoke vs. load

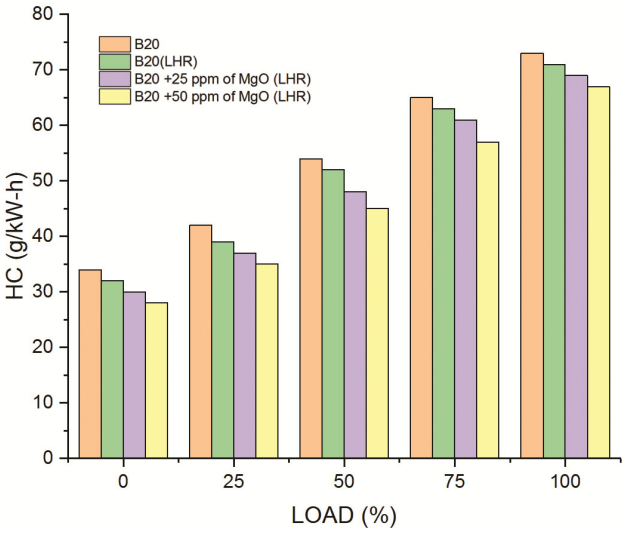

Fig. 9 — Plot of hydrocarbon emission vs. load

and the accumulation of fuel particles in the crevice volumes of the combustion chamber. Also, the admission of surplus air inside the chamber often causes lean misfires, reduces the flame speed during combustion, and generates significant HC emissions. Fig. 9 depicts the relationship between hydrocarbons versus different loads for B20 with and without MgO nano additives. The results show that HC emissions have diminished by around 38.35%, 43.81%, and 46.26% for B20 (LHR), B20+25 ppm of MgO (LHR), and B20+50 ppm of MgO (LHR) compared to B20. It was found that using B20+50 ppm of MgO in an LHR engine significantly reduced HC emissions under all loads compared to other fuels. The LHR engine has lower flammability limitations and a shorter quenching distance. This reduction in unburned hydrocarbon emissions in the LHR engine is due to the upsurge of after-combustion temperature resulting from lower heat losses. Furthermore, biodiesel with MgO nanoparticle blends improved broad ignition inside the combustion chamber. This was achieved by reducing ignition delay time, improving the fuel outburst procedure, and increasing HRR during ignition. The calorific value of the MgO nanoparticle-based blend increases, resulting in proper fuel atomization and reduced HC emissions[19].

Smoke emission

The smoke opacity obtained from emissions for different loads for LHR and standard engines using various fuels is displayed in Fig. 10. The figure shows that fuel blends with conventional engines delivered higher smoke emissions at all load conditions. Specifically, the smoke emission is observed as 78.2% for the B20 fuel blend, whereas it is 76.3%, 74.3%, and 71.4% for the B20 (LHR), B20+25 ppm of MgO (LHR), and B20+50 ppm of MgO (LHR) fuel blends, respectively. The reduction in smoke emissions of the low heat rejection engine is attributed to higher temperatures in the combustion chamber. The coating of engine parts increases combustion efficiency, raising the temperature of both the engine parts and the combustion chamber. Consequently, engines exhibit reduced smoke opacity due to enhanced combustion resulting from turbulence and a homogenous air-fuel ratio in the combustion chamber, thanks to thermal barrier coatings[20]. Furthermore, the oxygenated content of magnesium oxide nanoparticles effectively improves

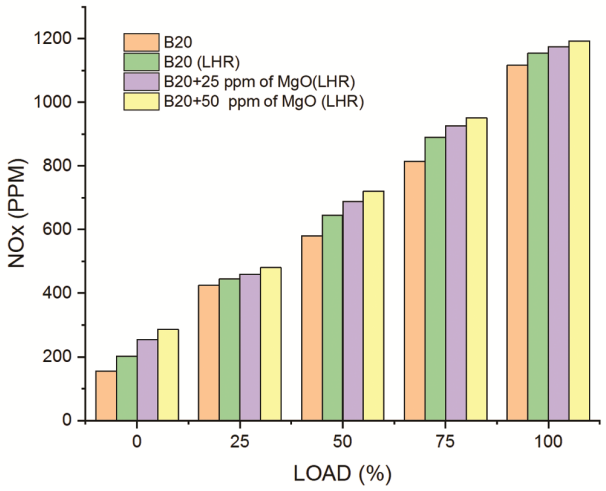

Fig. 11 — Plot of NO_x emission vs. load

combustion, reducing smoke emissions[21]. The dosage of 50 ppm of MgO with spirulina algae methyl ester on the TBC engine provides better results than all other fuel combinations.

Nitrogen oxide emission

The most harmful emissions from an engine exhaust are nitrogen oxides, caused by high oxygen availability in the cylinders and high temperatures inside the engine. Fig. 11 shows the fluctuation of NO_x emissions at different loads using various fuel blends. At maximum load, NO_x emissions from B20 fuel were observed at 1117 ppm. However, NO_x emissions from B20 (LHR), B20+25 ppm of MgO (LHR), and B20+50 ppm of MgO (LHR) fuel blends were 1154, 1175, and 1193 ppm, respectively. The figure indicates that nitrogen oxide emissions increase with increasing load. Biodiesel blends containing nano-additives produce more NO_x than B20. Several studies have reported that biodiesel has a slightly higher adiabatic flame temperature due to its oxygenated component. This aids complete combustion, raising the temperature and increasing NO_x emissions[22]. When the LHR engine runs, NO_x emissions rise with all fuel blends. The higher O_2 content in magnesium oxide with biodiesel blends and the thermally coated engine increases combustion temperatures, consequently elevating NO_x emissions.

Conclusion

This experiment employed spirulina algae methyl ester (B20) as fuel. MgO nanoparticles were included at 25 and 50 ppm and thoroughly mixed with the spirulina biodiesel for 45 min in an ultrasonicator. A low thermal conductivity material (lanthanum aluminate) was coated at about 200 microns thickness on the cylinder liners and piston heads. The performance, combustion, and emission characteristics of engines with and without coatings are investigated. Based on experimental results, LHR engines exhibit improved performance and combustion characteristics. Moreover, emissions characteristics such as CO, HC, and smoke have been reduced except the NO_x emissions.

References

1 Gad M S, El-Shafay A S & Abu H H M, *Process Saf Environ Prot*, 147 (2021) 518.
2 Pandey K K & Murugan S, *Int J Ambient Energy*, 43 (2022) 2486.
3 Parlak A, Yaşar H, Haşimoglu C & Kolip A, *Appl Therm Eng*, 25 (2005) 3042.
4 Haşimoglu C, Ciniviz M, Özsert I, Içingür Y, Parlak A & Salman M S, *Renew Energy*, 33 (2008) 1709.
5 Murugesan P, Balasubramanian D, Padmanabhan S, Murugunachippan N, Afzal A, Sharma P & Kiran K, *Process Saf Environ Prot*, 176 (2023) 1101.
6 Dhinesh B, Annamalai M, Lalvani I J & Annamalai K, *Appl Therm Eng*, 112 (2017) 627.
7 Krupakaran R L, Reddy V, Hariprasad T, Sachuthananthan B, Dhinesh B, Anchupogu P, Ratnakamala P & Saravanan V, *Int J Ambient Energy*, 44 (2023) 2250.
8 Elumalai P V, Parthasarathy M, Murugan M, Saravanan A & Sivakandhan C, *Int J Green Energy*, 18 (2021) 1482.
9 Chisti Y, *Biotechnol Adv*, 25 (2007) 294.
10 Arias M E, Knoot T G, Drennan C S & Dickson K L, *J Environ Manage*, 217 (2018) 211.
11 Hazar H, *Appl Energy*, 87 (2010) 134.
12 El-Seesy A I, Abdel-Rahman A K & Bady M, *Energy Convers Manage*, 135 (2017) 373.
13 Sivakumar E R, Senthilkumar P & Sreenivasan M, *Mater Today Proc*, 33 (2020) 675.
14 Jaikumar S, Srinivas V & Rajasekhar M, *Energy*, 224 (2021) 120197.
15 Krishna M V S M, Prakash T O & Ushasri P, *Renew Sust Energy Rev*, 53 (2016) 606.
16 Karishma S M, Rajak U & Naik B K, *Energy*, 245 (2022) 123304.
17 Karthickeyan V, *Renew Energy*, 148 (2020) 772.
18 Özgür M, Özcanli M & Aydin K, *Int J Green Energy*, 12 (2015) 51.
19 Senthil K S, Purushothaman K & Rajan K, *Therm Sci*, 21 (2017) 489.
20 Manigandan S, Sarweswaran R, Booma Devi P, Yasin S Kondratiev A,Venkatesh S, Rakesh Vimal M & Jensin Joshua S, 262 (2020) 116336.
21 Hoseini S S, Najafi G, Ghobadian B, Mamat R, Ebadi M T & Yusaf T, *Renew Energy*, 125 (2018) 283..
22 Öztürk U, Hazar H & Arı Y S, *Energy*, 186 (2019) 115871.